HHS Public Access

Author manuscript

Mol Cancer Ther. Author manuscript; available in PMC 2022 June 01.

Published in final edited form as:

Mol Cancer Ther. 2021 December ; 20(12): 2457–2468. doi:10.1158/1535-7163.MCT-21-0368.

IgE-based therapeutic combination enhances anti-tumor response in preclinical models of pancreatic cancer

Spas Dimitrov Markov[a], **Thomas C. Caffrey**[a], **Kelly A. O'Connell**[a], **James A. Grunkemeyer**[a], **Simon Shin**[a], **Ryan Hanson**[a], **Prathamesh P. Patil**[a], **Surendra K. Shukla**[a], **Daisy Gonzalez**[a], **Ayrianne J. Crawford**[a], **Krysten E. Vance**[a], **Ying Huang**[a], **Kirsten C. Eberle**[a], **Prakash Radhakrishnan**[a], **Paul M. Grandgenett**[a], **Pankaj K. Singh**[a], **Ragupathy Madiyalakan**[b], **Tracy R. Daniels-Wells**[c], **Manuel L. Penichet**[d], **Christopher F. Nicodemus**[e], **Jill A. Poole**[f], **Elizabeth M. Jaffee**[g], **Michael A. Hollingsworth**[a], **Kamiya Mehla**[a,*]

[a]The Eppley Institute for Research in Cancer and Allied Diseases, University of Nebraska Medical Center, Omaha, Nebraska, USA.

[b]OncoQuest Pharmaceuticals Inc. Edmonton, Alberta, Canada.

[c]Division of Surgical Oncology, Department of Surgery, University of California in Los Angeles (UCLA), USA.

[d]Division of Surgical Oncology, Department of Surgery and Department of Microbiology, Immunology and Molecular Genetics; The Molecular Biology Institute; Jonsson Comprehensive Cancer Center, University of California, Los Angeles (UCLA), California, USA.

[e]AIT Strategies, Franconia, New Hampshire, USA.

[f]Allergy and Immunology Division, Department of Internal Medicine, University of Nebraska Medical Center, Omaha, Nebraska, USA.

[g]Bloomberg–Kimmel Institute for Cancer Immunotherapy, Johns Hopkins University School of Medicine, Baltimore MD, USA.

Abstract

[*]Correspondence: Kamiya Mehla, Ph.D., 986805 Nebraska Medical Center, Omaha, NE, USA 68198-6805., kamiya.mehla@unmc.edu, 1-402-836-9117.

Authors' contributions

S. D. Markov: Investigation, formal analysis, data curation, methodology, writing-editing. **T. C. Caffrey**: Methodology, data curation, investigation, formal analysis and editing. **K. A. O'Connell**: Data curation, investigation and management of mice samples. **J. A. Grunkemeyer**: Investigation and management of mice samples. **S. Shin**: Investigation and data curation. **R. Hanson**: Data curation and formal analysis. **P. P. Patil**: Investigation and data curation. **S. K. Shukla**: Investigation and data curation. **D. V. Gonzalez**: Investigation and data curation. **A. J. Crawford**: Data curation**. K. E. Vance:** Data curation. **Y. Huang**: Investigation. **K. C. Eberle**: Management of human samples. **P. Radhakrishnan**: Investigation and writing-review-editing. **P. M. Grandgenett**: Resources and funding. **P. K. Singh**: Resources, supervision, funding and writing-review-editing. **R. Madiyalakan**: Conceptualization, resources and writing-review-editing. **T. R. Daniels-Wells**: Writing-review-editing. **M. L. Penichet:** Writing-review-editing. **C. F. Nicodemus**: Conceptualization and writing-review-editing. **J. A. Poole**: Funding, resources, methodology and writing-review-editing **E. M. Jaffee**: Conceptualization, and writing-review-editing. **M. A. Hollingsworth:** Conceptualization, Supervision, funding, resources and writing-review-editing. **K. Mehla:** Conceptualization, supervision, funding, investigation, methodology, formal analysis, writing original draft, and writing-review-editing.

Conflicts of interest

Dr. Ragupathy Madiyalakan is an employee and owns shares of OncoQuest pharmaceuticals Inc. Dr. Christopher Nicodemus is a paid advisor to the OncoQuest pharmaceuticals Inc. A total of four patents on MUC1.IgE have been assigned to OncoQuest Pharmaceuticals Inc.

Pancreatic ductal adenocarcinoma (PDAC) represents 3% of all cancer cases and 7% of all cancer deaths in the United States. Late diagnosis and inadequate response to standard chemotherapies contribute to an unfavorable prognosis and an overall 5-year survival rate of less than 10% in PDAC. Despite recent advances in tumor immunology, tumor-induced immunosuppression attenuates the immunotherapy response in PDAC. To date, studies have focused on IgG-based therapeutic strategies in PDAC. With the recent interest in IgE-based therapies in multiple solid tumors, we explored the MUC1-targeted IgE antibody's potential against pancreatic cancer. Our study demonstrates the notable expression of FcεRI (receptor for IgE antibody) in tumors from PDAC patients. Our study showed that administration with a limited amount of MUC1 targeted-IgE (mouse/human chimeric anti-MUC1.IgE) antibody at intermittent levels in combination with checkpoint inhibitor (anti-PD-L1) and TLR3 agonist (PolyICLC) induces a robust anti-tumor response that is dependent on NK and CD8 T cells in pancreatic tumor-bearing mice. Subsequently, our study showed that IgE antibody's antigen specificity plays a vital role in executing the anti-tumor response as non-specific IgE, induced by ovalbumin (OVA), failed to restrict tumor growth in pancreatic tumor-bearing mice. Utilizing the OVA-induced allergic asthma-PDAC model, we demonstrate that allergic phenotype induced by OVA cannot restrain pancreatic tumor growth in orthotopic tumor-bearing mice. Together, our data demonstrate the novel tumor protective benefits of tumor antigen-specific IgE-based therapeutics in a preclinical model of pancreatic cancer, which can open new avenues for future clinical interventions.

Introduction

Pancreatic ductal adenocarcinoma (PDAC) is one of the most lethal malignancies. Approximately 49,000 people will die of PDAC in 2022 (1). Late diagnosis and chemo-resistance underlie the reduced survival rate of 10% (2). Unlike other solid tumors, PDAC has proven to be refractory, primarily to single-agent immunotherapeutic approaches (3–5). These studies suggest that more profound immunosuppression exists in pancreatic cancer compared to other solid tumors (6, 7). Thus, multi-pronged therapeutic strategies are expected to overcome the immunosuppressive microenvironment and provide superior survival benefits for pancreatic cancer patients. The current immunotherapeutic strategies against PDAC primarily focus on checkpoint blockades to activate CD8 T cells. However, ipilimumab or tremelimumab checkpoint blockades demonstrated only a partial response in clinical trials when combined with gemcitabine. Notably, a granulocyte-macrophage colony-stimulating factor (GM-CSF) gene-transfected tumor cell vaccine (GVAX) improved PDAC patient disease-free survival (DFS) when combined with radiotherapy or 5-FU-based chemoradiation in phase I and Phase II trials, respectively (8–10). However, other immunotherapies, including DNA or peptide vaccines, have failed to demonstrate clinical benefits in PDAC patients. All these immunotherapeutic approaches have largely ignored other immunosuppressed innate immune players, such as natural killer cells (NK), that are not MHC-restricted and respond to tumor insults by generating IFN-γ for T cell activation. While NK cell-based therapeutics have shown some promising efficacies against hematologic malignancies (11), the success of these strategies is yet to be examined against solid tumors. To date, only a few NK cell-targeted strategies have been employed in the preclinical models for solid tumors (12, 13). Hence the therapeutic combination that boosts

both cytotoxic T cell (CTL)- and NK cell-mediated antitumor response has not yet been studied and may provide long-lasting therapeutic benefits in PDAC.

Epidemiological evidence suggests that individuals with allergies have a lower incidence of pancreatic cancer (14, 15). This indicates that distinct immune surveillance underlies protection against pancreatic cancer observed in allergic individuals (16). A previous study reported the existence of tumor-antigen-specific IgE antibodies in the serum of PDAC patients. Interestingly, these patients did not exhibit any allergic symptoms. Also, IgE isolated from the serum of PDAC patients showed peripheral blood mononuclear cell-mediated antibody-dependent cell cytotoxicity (ADCC) against human pancreatic cancer cells (HPACs) in *ex vivo* assays (17). Additionally, a Phase I clinical trial of MOv18 IgE (IgE antibody targeting the folate receptor alpha) has shown anti-tumor benefits in advanced cancers (18). Given the myriads of immune cells expressing IgE receptor, we hypothesized that therapeutic targeting of tumor antigens with IgE antibody would provide robust anti-tumor benefits against pancreatic cancer.

MUC1 is a critical therapeutic target in solid tumors, whose C-terminal domain contributes to immune evasion (19). To date, successful MUC1-based immunotherapies have remained elusive. Hence, we investigated a MUC1-targeted IgE antibody (mouse/human chimeric anti-MUC1.IgE) in combination with Toll-like receptor 3 (TLR3) agonist (PolyICLC) and anti-PD-L1 against pancreatic tumors in double transgenic (dTg) mice that express human MUC1 and human IgE antibody receptor (FcεRIα). Our study demonstrated that anti-MUC1.IgE + anti-PD-L1 + PolyICLC combination promotes NK and CD8 T-cell mediated antigen-specific immune responses that restrict pancreatic tumor growth in an otherwise immunosuppressed preclinical model of PDAC. We also noted that this combination promoted MUC1 antigen cross-presentation to CD8 T cells and NK cell-mediated tumor killing in *ex vivo* assays. Of note, we also demonstrate that Ovalbumin (OVA)-induced IgE is inefficient in controlling tumor growth in the PDAC model. Overall, these studies will open new avenues for IgE-based therapeutics against pancreatic cancer.

Material and Methods

Mice and cells lines

hMUC1/hFcεRIα C57BL/6J dTg mice were generated by breeding hMUC1single Tg mice and hFcεRIα single Tg mice. hMUC1 Tg mice have been described earlier (20). hFcεRIα Tg mice (stock no: 010506) were purchased from Jackson laboratory. Panc02.MUC1 (expressing human MUC1), Panc02.Neo and KPC.MUC1 (expressing human MUC1) cells have been described earlier (20). All cell lines were authenticated from University of Arizona Genetics Core by STR profiling. C57BL/6-congenic KPC cells are derived from the spontaneous PDAC model with Kras and p53 mutations. All animal studies included equal number of male and female mice. All the animal studies were conducted in accordance with, and with the approval of the Institutional Animal Care and Use Committee (IACUC) guidelines. Mice were genotyped for FcεRIα and MUC1 expression using primers as mentioned in table 1.

Antibodies

CHO-K1–3C6 cell line expressing chimeric mouse/human anti-MUC1.IgE was provided by OncoQuest Pharmaceuticals Inc., Edmonton, AB, Canada) (21). Amino acid sequence for the heavy and light chain of anti-136 human MUC1.IgE-3C6 are shown in Supplementary Fig. S1. The cell line was cultured in Dulbecco's Modified Eagle Medium/Nutrient Mixture F-12 (DMEM/F12) media supplemented with 10% fetal bovine serum (FBS) and weaned to DMEM with 5% FBS. The murine myeloma cell line (SP2/0 Ag-14) expressing mouse/human chimeric anti-Prostate specific antigen (PSA).IgE (22) was a gift from OncoQuest Pharmaceuticals Inc. and was cultured in Isocove's Modified Eagle Medium (IMDM) with 5% FBS. The antibody conditioned culture supernatants were collected from above cell lines and filtered through 0.25μm PMSF filters. Anti-MUC1.IgE and anti-PSA.IgE conditioned media were eluted from a human IgE capture liquid chromatography column prepared with bound omalizumab (Xolair; Novartis Pharmaceuticals Ltd/Genentech, South San Francisco, CA). Subsequently, all antibody eluate peaks were dialyzed against 300 buffer changes of PBS in 10K MWCO Slide-A-Lyzer G2 dialysis cassettes (cat no: 87732, Thermo Fisher Inc., Waltham, MA). Dialysates were quantified by 280 nm absorbance via a NanoDrop One spectrophotometer. Western blot as well as ELISA confirmed antigenicity. Purified antibody lots were lyophilized for long-term storage. Murine monoclonal anti-human MUC1.IgG1 (AR20.5) antibody is described earlier (20).

Tumor model and antibody treatment

Panc02.MUC1 cells (1×10^6 cells/100μl) were challenged subcutaneously (subcute) between the scapulae in hMUC1/hFcεRIα dTg mice. Post challenge, mice were randomized into different experimental groups (Saline control; anti-PD-L1; PolyICLC; anti-MUC1.IgE; anti-PD-L1 + PolyICLC; anti-MUC1.IgE + anti-PD-L1; anti-MUC1.gE + PolyICLC; and anti-MUC1.IgE + PolyICLC + anti-PD-L1, n=8 mice per group), and treated with respective antibodies. Anti-PD-L1 was purchased from BioXcell (Cat: BE0101, BioXcell Inc., New Hampshire, USA), whereas OncoQuest Inc., provided PolyICLC for the animal studies. Post-treatment, mice were monitored for overall survival and tumor growth using established protocols (20). Tumor diameters (2/tumor) were measured weekly for tumor volume measurement (V= (length x width^2)1/2). Mice were euthanized as per the IACUC requirements. For orthotopic studies, KPC.MUC1 tumor cells (3×10^3 cells/30 μl) were implanted in the pancreas of eight- to nine-weeks-old immunocompetent hMUC1/hFcεRIα dTg mice using established protocols (23). Equal number of male and female mice were used in the study. Post-implantation mice were randomized into different experimental groups and treated with the respective antibodies and monitored for tumor growth (V= (length x width^2)1/2) using vernier calipers as per the institutional IACUC guidelines. In the OVA-PDAC model, KPC tumor cells (3×10^3 cells/30μl) were implanted in the pancreas of eight- to nine-weeks-old immunocompetent C57BL/6J mice. Subsequently, mice were monitored for tumor growth using ultrasound imaging with the Vevo 3100 system and euthanized on day 42 as per Insitituonal IACUC guidelines. Tumor volume was calculated using the Vevo LAB imaging software (VisualSonics Inc., Toronto, Canada) integrated in Vevo 3100 system. CD8, CD4, and NK cell depletion studies were performed as described in a previous study (20).

OVA challenges in pancreatic tumor model

C57BL/6J mice (JAX:000664) were sensitized and challenged to OVA as previously described with modifications (24). For sensitization, 20μg OVA was mixed with 2 mg of Al (OH)3 (Thermo Fisher Inc., Waltham, MA) in 0.2 ml saline and administered intraperitoneally. Non-sensitized animals received saline only. Mice were implanted with the tumor cells in the pancreas on days as mentioned in figure legend. Mice were challenged with nebulized 1.5% OVA in saline or saline alone (saline challenged groups), for 20 minutes twice a week until the end of the study. Allergic phenotype was validated by IgE quantitation in the serum using ELISA kit (cat no: 501128838, eBioscience Inc, CA, USA) as per the manufacturer's protocol. Bronchoalveolar lavage fluid (BALF) was collected from the airways and differential counting for eosinophil was performed on cytospin-prepared slides using DiffQuick (Siemens Healthineer Inc., Neward, DE) as previously described (24).

Immunohistochemistry (IHC) staining and Western blot analyses

Freshly harvested tumor tissues from tumor-bearing mice were processed for tumor-infiltrating lymphocytes (TILs) and IHC (formalin-fixed) analyses using established protocols (25). Tissue sections were stained for Ki67 and cleaved caspase-3. All the antibodies are described in table 2. Stained slides were imaged using a Leica microscope equipped with a LAS-AF processing system and quantitated using ImageJ software (24). PDAC and metastasis tumor tissue slides were acquired through RAPID autopsy program at UNMC and stained for FcεRI antibody (LS-B3150). Stained slides were quantitated blindly by lab technician using a formula, histological score = [1 x (% cells 1+) + 2x (% cells 2+) + 3x (% cells 3+)], where 1+, 2+, and 3+ corresponds to weak, moderate, and strong staining intensity respectively, as described previously (26).

Anti-MUC1.IgE binding assay

MUC1 specific binding ability of anti-MUC1.IgE antibody was confirmed using Panc02.MUC1 in the *in vitro* assay. Here, Panc02.MUC1 were incubated with or without anti-MUC1.IgE antibody for 12 hr. Post-incubation, cells were harvested and stained for epsilon (ε) and kappa (κ) chains using florescent conjugated anti-epsilon (ε) (goat anti-human IgE Fc-FITC) and anti-kappa (κ) (anti-human kappa APC) antibodies.

Immunological assays

Antigen peptide uptake assay for dendritic cells (DCs) using FITC-MUC1 peptide was performed as previously described (27). For the assay, FITC-MUC1 peptide (Hi Lyte Fluor 488-GVTSAPDTRPAPGSTA-OH) was custom synthesized (AnaSpec Inc., Fremont CA). ELISpot assay was performed using mouse IFN- γ ELISpot kit (cat no: EL485, RnD Systems, Inc., Minneapolis, MN) as per manufacturer's protocol. CFSE-based proliferation assay was utilized to measure CD8 T cell proliferation upon co-culture with antigen-antibody loaded DCs using established protocols (27). CD107a-based degranulation assay was performed to determine the functional activity of NK cells, as described previously (28).

Expression of Fc-Receptors in PDAC subtypes

PDAC normalized expression data from Bailey et al. was collected and boxplots plotted for each pancreatic subtype using Matlab (MATLAB, RRID:SCR_001622) (29). Outliers are plotted as data points that reside approximately 2.7 standard deviations beyond the mean expression. Statistical analysis comparing PDAC subtypes was performed using one-way ANOVA for multiple comparisons. Primary pancreatic tumor tissues were procured through institutional RAPID autopsy program. Freshly harvested tumor tissues were minced into small pieces and incubated in digestion buffer (complete DMEM containing 2% Collagenase A (Roche 11284932001) and 0.25 U/ml of DNAse I (Roche 11284932001 for 20 mins at 37°C with constant shaking. Subsequently, the digest was filtered through a 70μm nylon strainer and centrifuged at 2000 rpm for 5 mins. Finally, the cells were washed with 1x PBS and stained with live/dead dye. Post staining, cells were washed with buffer (1 x PBS with 0.5% BSA) and stained with fluorescent conjugated antibodies corresponding to different immune cell subsets. Samples were acquired by BD Bioscience LSRII flow cytometer and data was analyzed by FlowJo Version 8.8.7 software by TreeStar.

Statistical analyses

Survival differences were plotted using Kaplan-Meier plots and differences between experimental groups were assessed using log-rank tests. Tumor volume measurements over time were compared using two-way ANOVA analyses with repeated measurement (Bonferroni post-hoc test). The percentage of immune subsets in different mice subsets was measured using one-way ANOVA with a Bonferroni post-test adjustment for multiple measurements in Prism 6 software (GraphPad Prism, RRID:SCR_002798, GraphPad Software Inc., San Diego, CA). All the p values ≤ 0.05 were considered significant.

Results

Pancreatic tumors harbor FcεRIα chain-expressing cells.

The FcεRI receptor is a high-affinity IgE receptor that consists of one α subunit, one β subunit, and two γ subunits in mice and human. In humans, FcεRI can also exists in an alternate trimeric form ($\alpha\gamma_2$) (30). While the extracellular domain of the α subunit binds to IgE heavy chain, the β and γ subunits relay the signal to downstream pathways (31). To examine the feasibility of IgE-based therapeutics, we first determined the FcεRI expression in pancreatic tumor tissues. In our study (Fig. 1A), the normal tissue adjacent to the tumor displays a notable expression of FcγRIII and FcεRI. While FcγRIII, also known as CD16, is a receptor for monomeric IgG-type antibodies, FcεRI binds to the Fc region of IgE antibody isotype with high affinity (32). Next, we investigated the expression of IgG and IgE receptor genes (*FCER1A, FCER1G, FCGR3A,* and *FCGR1A*) in different subtypes of PDAC by using previously published expression data (29). Herein, we noted significant enrichment of the *FCGR3A* in the squamous subtype of PDAC (Fig. 1B). Similarly, *FCER1G* displayed a significant enrichment in the squamous subtype of PDAC. In contrast, *FCER1A* demonstrated a uniform expression, albeit low compared to *FCGR3A*, in all the subtypes of PDAC. Subsequently, we assessed the cell types that express FcεRIα subunit in the pancreatic tumor by using a flow cytometer. Herein, we noted the abundance of FcεRIα positive mast cells, monocytes, and a small fraction of eosinophils inside the pancreatic

tumor (Fig. 1C–D, Supplementary Fig. S2). Subsequently, we assessed the expression of FcεRI in the primary tumor and matched liver metastatic tissue specimens. Our study demonstrated a significant upregulation of FcεRI expression in primary tumors as compared to the normal pancreas. In contrast, we did not observe a significant difference in FcεRI expression between the primary tumors and metastatic liver lesions (Fig. 1E).

Anti-MUC1.IgE + anti-PD-L1 + PolyICLC combination improved the survival of pancreatic tumor-bearing mice in dTg mice.

Upon confirmation of FcεRI expression in PDAC tumors, we examined the therapeutic efficacy of mouse/human chimeric anti-MUC1.IgE antibody in the preclinical model of PDAC by utilizing hMUC1/hFcεRIα dTg mice (21). Our antibody targets the PDTRPAP sequence in the tandem repeat of the human MUC1 antigen (Fig. 2A). This antibody specifically binds to the MUC1 antigen on pancreatic tumor cells (Fig. 2C–D). Furthermore, our data demonstrate FcεRIα expression on mast cells, DCs, but not on T cells in dTg mice (Fig. 2D). Next, we investigated the therapeutic efficacy of anti-MUC1.IgE in combination with the TLR3 agonist (PolyICLC) and a checkpoint inhibitor (anti-PD-L1) against subcutaneous Panc02.MUC1 tumors (Fig. 2E). This combination is based on previously published data where we demonstrated improved efficacy of anti-MUC1.IgG1 isotype in combination with PolyICLC and anti-PD-L1 against PDAC tumors (20). In our pilot experiment, three single intraperitoneal injections (i.p.) of anti-MUC1.IgE (40μg) to healthy dTg mice at 10 days interval did not display any adverse effects, such as anaphylactic shock in mice. In our *in vivo* study, a significant proportion of anti-MUC1.IgE + PolyICLC + anti-PD-L1-treated mice rejected Panc02.MUC1 and remained tumor-free. Overall, anti-MUC1.IgE-based triple combination-treated mice displayed increased survival as compared to saline-treated control mice. Furthermore, anti-MUC1.IgE-combination-treated mice that failed to reject tumor displayed significantly attenuated tumor growth compared to other treatment groups (Fig. 2F–G). Next, we performed a tumor re-challenge experiment by implanting Panc02.Neo control and Panc02.MUC1 tumor cells on the opposite flanks of anti-MUC1.IgE-combination-treated tumor-free mice. We monitored these mice for tumor rejection and tumor growth over time. Herein, unchallenged treatment-naïve dTg animals served as controls (Fig. 2H). Panc02.Neo and Panc02.MUC1 cell lines exhibit indistinguishable growth rates in the *in vitro* system (20). In our experiment, we did not see the rejection of Panc02.MUC1 and Panc02.Neo tumor cells upon re-challenge in previously anti-MUC1.IgE-combination-treated tumor-free mice. However, these mice demonstrated a significantly slower growth rate of Panc02.MUC1 tumors compared to Panc02.Neo tumors (Fig. 2I). Contrastingly, both the tumors grew at indistinguishable rates in treatment-naïve dTg mice. Overall, our data demonstrate that anti-MUC1.IgE + PolyICLC + anti-PD-L1 combination provides a MUC1 specific immune response that delays tumor appearance and hinders tumor growth in heterotopic models.

Anti-tumor efficacy of anti-MUC1.IgE + anti-PD-L1 + PolyICLC combination in orthotopic tumor-bearing dTg mice but not in single Tg mice.

Next, we assessed the therapeutic benefits of anti-MUC1.IgE-based combination in an aggressive model of PDAC, which mimics the pathological features of human PDAC (33). We utilized KPC.MUC1 tumor cells and employed anti-human PSA.IgE (22) as a

control for our studies as prostate antigen (PSA) is not present in pancreatic tumors. In our study, treatment with anti-MUC1.IgE + anti-PD-L1+ PolyICLC combination significantly delayed tumor growth and prolonged survival of orthotopic tumor-bearing dTg mice compared to control mice (Fig. 3A–B). Furthermore, anti-MUC1.IgE-based combination significantly reduced tumor burden and provided superior survival benefits compared to anti-PD-L1 + PolyICLC and anti-PSA.IgE + anti-PD-L1 + PolyICLC treatments (Fig. 3C–D). Interestingly, anti-MUC1.IgE + anti-PD-L1 + PolyICLC combination displayed an improved, but not significant, anti-tumor response as compared to anti-MUC1.IgG1-based combination. The above data suggest that while anti-MUC1.IgG1 and anti-MUC1.IgE-combination triggers similar anti-tumor pathways, anti-MUC1.IgE activates additional anti-tumor players that contribute to improved therapeutic benefits. To further dissect the critical role of FcεRIα-MUC1 in the underlying anti-tumor response of anti-MUC1.IgE, we examined the efficacies of anti-MUC1.IgE and anti-MUC1.IgG1(AR20.5)-based combination in different transgenic mice, i.e., hFcεRIα single transgenic (Tg) and hMUC1 single Tg mice. As hFcεRIα Tg mice do not express human MUC1, we utilized KPC cells without human MUC1 in an orthotopic implantation study. Contrastingly, hMUC1 Tg mice were implanted with KPC.MUC1 cells. Given the absence of hMUC1 antigen in hFcεRIα Tg mice, tumor growth rates were indistinguishable in all the treatment groups. Importantly, anti-MUC1.IgE-based combination exhibited tumor protective benefits only in hMUC1/hFcεRIα dTg mice. In the absence of FcεRIα, anti-MUC1.IgE-based combination displayed attenuated anti-tumor response in hMUC1Tg mice (Fig. 3E–F). Hence, the requirement of the FcεRIα–dependent pathway underlies the improved therapeutic efficacy of anti-MUC1.IgE-based combination over anti-MUC1.IgG1-based therapy in pancreatic tumor-bearing dTg mice. Next, our study demonstrated that anti-MUC1.IgE-based combination treatment significantly attenuated the tumor cell proliferation in treated mice (Fig 3G–H). Interestingly, anti-MUC1.IgE-based combination treatment also showed a trend toward increased apoptosis of tumor cells in the treated mice as compared to controls (Fig. 3H).

NK and CD8 T cell depletion reduced the efficacy of anti-MUC1.IgE-based combination in tumor-bearing mice.

Next, we interrogated the key immune subsets that underlie the therapeutic efficacy of anti-MUC1.IgE + PolyICLC + anti-PD-L1 combination. Elimination of NK and CD8 T cells reduced the survival of anti-MUC1.IgE-combination treated Panc02.MUC1 subcute and KPC.MUC1 orthotopic (ortho) tumor-bearing mice (Fig. 4A–B). Previously, anti-MUC1.IgG1-based combination showed CD8 T-mediated anti-tumor response against pancreatic cancer in MUC1.Tg mice (20). Hence, we compared the efficacy of anti-MUC1.IgG1 and anti-MUC1.IgE-based combination therapy in the presence or absence of NK cells in dTg mice. NK cell depletion did not alter the anti-tumor response of anti-MUC1.IgG1 + anti-PD-L1+ PolyICLC treatment, but significantly attenuated the prolonged survival benefits of anti-MUC1.IgE-based combination therapy in orthotopic tumor-bearing mice (Fig. 4C). Surprisingly, the tumor-infiltrating lymphocytes (TILs) assessment showed that anti-MUC1.IgE + anti-PD-L1 + PolyICLC does not alter the total number of NK and CD8 T cells. However, this combination significantly reduces the proportion of PD-1^{+} $TIGIT^{+}$ NK cells in treated tumors compared to other control counterparts (Fig. 4D).

Additionally, our study showed a significant increase in $CD103^+$dendritic cells (DCs), but no significant alteration in macrophages and MDSCs percentages in anti-MUC1.IgE + anti-PD-L1 + PolyICLC treated tumors compared to other groups. $CD103^+$DCs are conventional type cDC1s that cross-present tumor antigens to the CD8 T cells (34). As DCs also express FcεRI receptors we posit that increased $CD103^+$DCs in anti-MUC1.IgE-combination treated mice indicate DC-mediated activation of CD8 T cells. To support this idea, we performed an antigen-antibody immune complex uptake assay using FITC labeled MUC1 peptide (16-mer containing PDTRPAP sequence) and anti-MUC1.IgE antibody. Our data demonstrate increased uptake of peptide-antibody uptake by DCs and increased proliferation (CFSE dilution) of CD8 T cells upon incubation with immune complex-loaded DCs (Fig. 4E–F). In parallel, we demonstrated increased CD8 T cell activity (IFN-γ production) from the spleen of anti-MUC1.IgE + anti-PD-L1+ PolyICLC mice upon incubation with KPC.MUC1 cells in the *ex vivo* ELISpot assay (Fig. 4G). Additionally, we assessed the splenic NK function in the *ex vivo* CD107a-based degranulation assays. Extracellular appearance of CD107a, (LAMP1), suggests the fusion of lysosome with the plasma membrane in NK cells, transporting lytic granule outside for cytotoxic killing of target cells (35). Notably, NK cells from anti-MUC1.IgE + anti-PD-L1 + PolyICLC mice demonstrated increased degranulation as compared to control mice (Fig. 4H–I). Altogether, our data explain that while both anti-MUC1.IgG1 and anti-MUC1.IgE promoted CD8 T-cell-mediated efficacy, additional enhancement of NK cell activity provided improved (but not significant) therapeutic efficiency of anti-MUC1.IgE + PolyICLC + anti-PD-L1 against pancreatic cancer.

OVA-induced IgE does not attenuate tumor burden in OVA-challenged pancreatic tumor-bearing mice

Earlier, meta-analysis studies suggested an inverse relationship between allergy and the incidence of pancreatic cancer (14, 15). However, it is not known if IgE antibodies generated in response to allergic reactions can mount an immune response against the pancreatic tumor antigens. To determine the role of allergen-induced IgE responses, we investigated tumor growth of KPC mouse-derived tumor cell line before and after the sensitization and aerosol challenges with ovalbumin in OVA-induced allergic model (Fig. 5A, G). OVA challenges significantly increased circulating IgE in both naïve and pancreatic tumor-bearing mice compared to saline-challenged control mice (Fig. 5B, H). Furthermore, we noted increased proportion of eosinophils in the bronchial alveolar lavage (BAL) fluid of OVA-challenged tumor-bearing mice but not in control counterparts (Fig. 5C, 5I). However, there was no impact of OVA-induced IgE on the growth of the pancreatic tumor in the preclinical model of pancreatic cancer. There was no significant difference in the pancreatic tumor growth, weight, and volume between saline and OVA-challenged mice in both the early- and late-tumor models (Fig. 5D–F, J–L). Together, our data imply that OVA-induced IgE is ineffective in limiting pancreatic tumor growth in preclinical model of pancreatic tumor in immunocompetent C57BL/6J mice. Hence, our data suggest the significance of tumor-specificity of IgE antibodies in controlling pancreatic tumor growth.

Discussion

Multiple studies have highlighted the potential of IgE-based therapeutics in cancer. While anti-HER2/*neu* IgE significantly prolongs the survival of D2F2/E2 tumor-bearing Tg hFcεRIα mice, anti-PSA.IgE substantially extends the survival of hFcεRIα mice harboring CT26-PSA tumors (22, 36). Also, chimeric mouse/human anti-MOv18 IgE (anti-folate receptor αIgE) combined with human PBMCs prolongs the survival of ovarian cancer xenograft-bearing mice (37). Recently, clinical data from the Phase I trial demonstrate that anti-MOv18.IgE is well tolerated; only minor toxicities including, urticaria, were seen among the anti-MOv18.IgE-treated patients (18). In PDAC patients, tumor antigen-specific IgE in peripheral circulation is already reported (17). More recently, a study showed a significant accumulation of IgE^+ memory B cells and IgE antibodies in the pancreatic tumors of KPC mice (38). Taken this, we interrogated the potential utilization of tumor antigen-specific IgE against pancreatic cancer in the preclinical model of PDAC, which has not been examined so far.

The present study demonstrated the uniform expression of the FcεRI receptor in primary pancreatic and metastatic tumors. Our study verified the expression of FcεRIα subunit of the FcεRI on $CD14^+$ monocytes, mast cells, and eosinophils in primary pancreatic tumors. Subsequently, we demonstrated FcεRIα expression on mast cells and DCs in hMUC1/hFcεRIα dTg mice. Next, we demonstrated that anti-MUC1.IgE+anti-PD-L1+PolyICLC combination induced MUC1-specific cellular immune responses that mediate rejection of Panc02.MUC1 tumors in a subcutaneous model of PDAC. Anti-MUC1.IgE, utilized here, recognizes the tandem repeat domain of human MUC1 and binds to the corresponding human FcεRIα subunit of the FcεRI receptor (21). In addition, we demonstrated that anti-MUC1.IgE + anti-PD-L1+ PolyICLC significantly restricted the growth of KPC.MUC1 orthotopic tumors as compared to anti-PD-L1 + PolyICLC and anti-PSA.IgE + anti-PD-L1 + PolyICLC treatment. Anti-PD-L1 and PolyICLC combination has previously been shown to restrict the growth of solid tumors, including melanoma (39). Interestingly, the addition of anti-MUC1.IgE to anti-PD-L1 and PolyICLC combination further enhances the anti-tumor immunity as depicted by attenuated tumor burden in triple combination-treated tumor-bearing mice. Noteworthy, we did not observe any rejection of orthotopic tumors with anti-MUC1.IgE-based combination treatment. Compared to subcutaneous tumors, C57BL/6-congenic KPC tumor cell-derived orthotopic tumors exhibit rapid proliferation, which provides a smaller time window for therapeutic combinations to be efficacious. Furthermore, the extensive desmoplasia in orthotopic models may somewhat decrease the entry of therapeutics into the tumor. Our study further demonstrated the critical importance of tumor-targeted specificity of IgE-FcεRIα interaction by showing the efficacy of IgE-based therapy in tumor-bearing dTg mice but not in hMUC1Tg and hFcεRIαTg mice. Tumor protective benefits of anti-MUC1.IgE requires both the MUC1 antigen and FcεRIα receptor in our preclinical model. Earlier, we reported the efficacy of anti-MUC1.IgG1, in combination with anti-PD-L1 + PolyICLC in the preclinical model of PDAC (20). Anti-MUC1.IgG1, used in the previous study, is a mouse antibody that targets the DTRPAP sequence in the tandem repeat of extracellular MUC1 protein. Interestingly, anti-MUC1.IgE (mouse/human chimeric) also targets the same sequence in MUC1. Upon

comparison, anti-MUC1.IgE-based combination therapy demonstrated moderately improved anti-tumor immunity as compared to anti-MUC1.IgG1-based combination in dTg mice. Both IgE and IgG combinations utilize anti-tumor CD8 T cell responses. It is noteworthy that while intratumoral CD8 T cells were comparable between anti-MUC1.IgG1 and anti-MUC1.IgE combination-treated tumors, a significant increase in the proportion of $CD103^+$DCs were observed in the tumors from anti-MUC1.IgE combination-treated mice. It is well established that DCs express FcεRIα and cross-present antigens to CD8 T cells (27). Our study also showed that splenic DCs from dTg mice could take up anti-MUC1.IgE-MUC1-peptide complex and stimulate CD8 T-cell proliferation. Hence, our data suggest that $CD103^+$DC-CD8 T-cell interactions underlie the cell-mediated immune response of anti-MUC1.IgE + anti-PD-L1+ PolyICLC treatment.

In this report, we demonstrate an additional component of NK cell activity in anti-MUC1.IgE combination-treated mice. NK cell depletion abrogated the therapeutic efficacy of anti-MUC1.IgE- but not anti-MUC1.IgG1-based combination in pancreatic tumor-bearing mice. While the total proportion of NK cells remained unaltered, our study showed a significant drop in the $TIGIT^+$ and $PD\text{-}1^+$ NK cells in anti-MUC1.IgE combination-treated tumors compared to control counterparts. PD-1 and TIGIT are checkpoint inhibitors that are common between CD8 and NK cells (40). TIGIT restricts NK cell function, and blockade of TIGIT increases the anti-tumor response of NK cells against trastuzumab-coated breast cancer cells (41, 42). Thus, our data suggest that anti-MUC1.IgE-based combination increases NK cell activity in pancreatic tumor-bearing mice. Macrophages and DCs can regulate NK cell function (43, 44). As such, macrophages and DCs express FcεRIα (45). In an earlier report, anti-MOv18.IgE treatment has been shown to modulate the behavior of macrophages toward the anti-tumor phenotype (46). Surprisingly, previous studies 570 have not explored the effect of IgE on NK cells in their *in vivo* model. Hence our study is novel in demonstrating the therapeutic benefits of IgE-based therapy in enhancing NK cell-mediated anti-tumor response in the preclinical model of PDAC. Our data warrants further investigations to understand the mechanism that underlies NK cell-mediated anti-tumor response in anti-MUC1.IgE + anti-PD-L1+ PolyICLC treated tumor-bearing mice.

Next, our study shows that the antigen specificity of IgE play a vital role in executing the anti-tumor response as non-specific IgE, induced by OVA, failed to restrict tumor growth in the preclinical model of PDAC. Furthermore, our data demonstrate that pancreatic tumor burden does not alter OVA-induced IgE levels in the circulation. Our findings in the OVA-induced allergic asthma-PDAC model in mice contrast to the epidemiological studies suggesting that allergic phenotype could reduce the risk of developing pancreatic cancer. Interestingly, another *in vivo* study demonstrates that OVA-induced allergic inflammation does not impact the growth of carcinogen-induced lung tumorigenesis in BALB/c mice (47). It is important to highlight that while our study is limited to only OVA-induced acute model of asthma, epidemiological studies gathered evidences from the myriad of allergic diseases, including hay fever, skin allergy, and allergic rhinitis (14). Furthermore, though OVA-based models are frequently used to study pulmonary inflammation in mice, OVA is scarcely implicated in triggering human asthma (48). Moreover, the OVA-challenged mice exhibit an altered pattern of pulmonary inflammation, which is variant from that found in asthmatic individuals (49). Given the limitations of the OVA-based asthma model, other

murine models of allergen-induced disease, including the house dust mite, cockroach, or alternaria model, might shed additional insight into the relationship between allergy/asthma conditions and risk of developing PDAC. Nonetheless, we successfully demonstrate that OVA-induced IgE (non-specific IgE) is ineffective in restricting pancreatic tumor growth in immunocompetent mice. Moreover, our study provides crucial data on the pancreatic tumor growth in OVA-sensitized/challenged mice, which will provide a foundation for future investigations to understand the cross-talk between allergy and PDAC.

In conclusion, our study provides direct evidence that anti-MUC1.IgE has anti-tumor activity in the preclinical model of pancreatic cancer, and both the NK cell and T cell axis contribute to the effect in this system. The NK cell effect was unexpected and hence needs further evaluation in the context of both other models of IgE and cancer.

Supplementary Material

Refer to Web version on PubMed Central for supplementary material.

Acknowledgments

We would like to thank the University of Nebraska Medical Center Rapid Autopsy Pancreatic Program and the patients who generously donated their samples. We would also like to thank Jonathan Pester for his help in the pilot animal experiments. Besides, we would like to thank Camila G Pacheco and Amy J Nelson for their technical help in the animal studies.

K. Mehla is supported by NCI-SPORE P50 CA127297 Career Development Award. This study was also funded in part by the support of grants from the National Institutes of Health grant under the project numbers R01CA163649, R01CA210439, and R01CA216853 to **P. K. Singh** and R01CA181115 to **M.L. Penichet**, the Specialized Programs for Research Excellence (SPORE, NCI) under the project number 2P50 CA127297 to **M. A. Hollingsworth** and **P. K. Singh**, NCI Research Specialist award (5R50CA211462) to **P. M. Grandgenett** and the Pancreatic cancer detection consortium U01CA210240 to M. A. Hollingsworth. This work is also supported by grants from the National Institute of Environmental Health Sciences (R01ES019325) and National Institute for Occupational Safety and Health (U54OH010162) to **J. A. Poole**.

This study was also funded in part by the support of award from OncoQuest Pharmaceuticals Inc.

References

1. Cancer statistics, 2022. CA Cancer J Clin. 2022;72(1):7–33. [PubMed: 35020204]
2. American Cancer Society. Cancer Statistic. 2020, January 8.
3. Yarchoan M, Johnson BA, 3rd, Lutz ER, Laheru DA, and Jaffee EM. Targeting neoantigens to augment antitumour immunity. Nat Rev Cancer. 2017;17(4):209–22. [PubMed: 28233802]
4. Foley K, Kim V, Jaffee E, and Zheng L. Current progress in immunotherapy for pancreatic cancer. Cancer Lett. 2016;381(1):244–51. [PubMed: 26723878]
5. Postow MA, Callahan MK, and Wolchok JD. Immune Checkpoint Blockade in Cancer Therapy. J Clin Oncol. 2015;33(17):1974–82. [PubMed: 25605845]
6. Ho WJ, Jaffee EM, and Zheng L. The tumour microenvironment in pancreatic cancer - clinical challenges and opportunities. Nat Rev Clin Oncol. 2020;17(9):527–40. [PubMed: 32398706]
7. Liudahl SM, Betts CB, Sivagnanam S, Morales-Oyarvide V, da Silva A, Yuan C, et al. Leukocyte Heterogeneity in Pancreatic Ductal Adenocarcinoma: Phenotypic and Spatial Features Associated with Clinical Outcome. Cancer Discov. 2021.
8. Sarantis P, Koustas E, Papadimitropoulou A, Papavassiliou AG, and Karamouzis MV. Pancreatic ductal adenocarcinoma: Treatment hurdles, tumor microenvironment and immunotherapy. World J Gastrointest Oncol. 2020;12(2):173–81. [PubMed: 32104548]

9. Kamath SD, Kalyan A, Kircher S, Nimeiri H, Fought AJ, Benson A 3rd, et al. Ipilimumab and Gemcitabine for Advanced Pancreatic Cancer: A Phase Ib Study. Oncologist. 2020;25(5):e808–e15. [PubMed: 31740568]
10. Aglietta M, Barone C, Sawyer MB, Moore MJ, Miller WH Jr., Bagala C, et al. A phase I dose escalation trial of tremelimumab (CP-675,206) in combination with gemcitabine in chemotherapy-naive patients with metastatic pancreatic cancer. Ann Oncol. 2014;25(9):1750–5. [PubMed: 24907635]
11. Lamb MG, Rangarajan HG, Tullius BP, and Lee DA. Natural killer cell therapy for hematologic malignancies: successes, challenges, and the future. Stem Cell Res Ther. 2021;12(1):211. [PubMed: 33766099]
12. Romee R, Cooley S, Berrien-Elliott MM, Westervelt P, Verneris MR, Wagner JE, et al. First-in-human phase 1 clinical study of the IL-15 superagonist complex ALT-803 to treat relapse after transplantation. Blood. 2018;131(23):2515–27. [PubMed: 29463563]
13. Gras Navarro A, Bjorklund AT, and Chekenya M. Therapeutic potential and challenges of natural killer cells in treatment of solid tumors. Front Immunol. 2015;6:202. [PubMed: 25972872]
14. Cotterchio M, Lowcock E, Hudson TJ, Greenwood C, and Gallinger S. Association between allergies and risk of pancreatic cancer. Cancer Epidemiol Biomarkers Prev. 2014;23(3):469–80. [PubMed: 24554712]
15. Gomez-Rubio P, Zock JP, Rava M, Marquez M, Sharp L, Hidalgo M, et al. Reduced risk of pancreatic cancer associated with asthma and nasal allergies. Gut. 2017;66(2):314–22. [PubMed: 26628509]
16. Gandini S, Lowenfels AB, Jaffee EM, Armstrong TD, and Maisonneuve P. Allergies and the risk of pancreatic cancer: a meta-analysis with review of epidemiology and biological mechanisms. Cancer Epidemiol Biomarkers Prev. 2005;14(8):1908–16. [PubMed: 16103436]
17. Fu SL, Pierre J, Smith-Norowitz TA, Hagler M, Bowne W, Pincus MR, et al. Immunoglobulin E antibodies from pancreatic cancer patients mediate antibody-dependent cell-mediated cytotoxicity against pancreatic cancer cells. Clin Exp Immunol. 2008;153(3):401–9. [PubMed: 18803764]
18. James Spicer BB, Montes Ana, Banerji Udai, Kristeleit Rebecca, Veal Gareth J., Corrigan Christopher, Till Stephen, Nintos George, Brier Timothy, Funingana Ionut G., Joo Ern Ang Kam Zaki, Griffin Annie, Barton Claire, Jones Paul, Mellor Sarah, Brook Susan, Stoddart Katie, Selkirk Christopher, Carroll Simon, Lentfer Heike, Woodman Natalie, Pope Amy, Pellizzari Giulia, Nakamura Mano, Ilieva Kristina M., Khiabany Atousa, Stavraka Chara, Gould Hannah, Chauhan Jitesh, Bax Heather, Pinder Sarah, Josephs Debra and Karagiannis Sophia. Phase 1 trial of MOv18, a first-in-class IgE antibody therapy for cancer. Cancer research. 2020;Abstract(AACR; Cancer Res 2020;80(16 Suppl):Abstract nr CT141).
19. Maeda T, Hiraki M, Jin C, Rajabi H, Tagde A, Alam M, et al. MUC1-C Induces PD-L1 and Immune Evasion in Triple-Negative Breast Cancer. Cancer Res. 2018;78(1):205–15. [PubMed: 29263152]
20. Mehla K, Tremayne J, Grunkemeyer JA, O'Connell KA, Steele MM, Caffrey TC, et al. Combination of mAb-AR20.5, anti-PD-L1 and PolyICLC inhibits tumor progression and prolongs survival of MUC1.Tg mice challenged with pancreatic tumors. Cancer Immunol Immunother. 2018;67(3):445–57. [PubMed: 29204701]
21. Teo PZ, Utz PJ, and Mollick JA. Using the allergic immune system to target cancer: activity of IgE antibodies specific for human CD20 and MUC1. Cancer Immunol Immunother. 2012;61(12):2295–309. [PubMed: 22692757]
22. Daniels-Wells TR, Helguera G, Leuchter RK, Quintero R, Kozman M, Rodriguez JA, et al. A novel IgE antibody targeting the prostate-specific antigen as a potential prostate cancer therapy. BMC Cancer. 2013;13:195. [PubMed: 23594731]
23. Shukla SK, Markov SD, Attri KS, Vernucci E, King RJ, Dasgupta A, et al. Macrophages potentiate STAT3 signaling in skeletal muscles and regulate pancreatic cancer cachexia. Cancer Lett. 2020;484:29–39. [PubMed: 32344015]
24. Warren KJ, Dickinson JD, Nelson AJ, Wyatt TA, Romberger DJ, and Poole JA. Ovalbumin-sensitized mice have altered airway inflammation to agriculture organic dust. Respir Res. 2019;20(1):51. [PubMed: 30845921]

25. Burrack AL, Spartz EJ, Raynor JF, Wang I, Olson M, and Stromnes IM. Combination PD-1 and PD-L1 Blockade Promotes Durable Neoantigen-Specific T Cell-Mediated Immunity in Pancreatic Ductal Adenocarcinoma. Cell Rep. 2019;28(8):2140–55 e6. [PubMed: 31433988]
26. Hirsch FR, Varella-Garcia M, Bunn PA Jr., Di Maria MV, Veve R, Bremmes RM, et al. Epidermal growth factor receptor in non-small-cell lung carcinomas: correlation between gene copy number and protein expression and impact on prognosis. J Clin Oncol. 2003;21(20):3798–807. [PubMed: 12953099]
27. Platzer B, Elpek KG, Cremasco V, Baker K, Stout MM, Schultz C, et al. IgE/FcepsilonRI-Mediated Antigen Cross-Presentation by Dendritic Cells Enhances Anti-Tumor Immune Responses. Cell Rep. 2015;10(9):1487–95. [PubMed: 25753415]
28. Shabrish S, Gupta M, and Madkaikar M. A Modified NK Cell Degranulation Assay Applicable for Routine Evaluation of NK Cell Function. J Immunol Res. 2016;2016:3769590. [PubMed: 27413758]
29. Bailey P, Chang DK, Nones K, Johns AL, Patch AM, Gingras MC, et al. Genomic analyses identify molecular subtypes of pancreatic cancer. Nature. 2016;531(7592):47–52. [PubMed: 26909576]
30. Turner H, and Kinet JP. Signalling through the high-affinity IgE receptor Fc epsilonRI. Nature. 1999;402(6760 Suppl):B24–30. [PubMed: 10586892]
31. Prussin C, and Metcalfe DD. 4. IgE, mast cells, basophils, and eosinophils. J Allergy Clin Immunol. 2003;111(2 Suppl):S486–94. [PubMed: 12592295]
32. van der Poel CE, Spaapen RM, van de Winkel JG, and Leusen JH. Functional characteristics of the high affinity IgG receptor, FcgammaRI. Journal of immunology. 2011;186(5):2699–704.
33. Hingorani SR, Petricoin EF, Maitra A, Rajapakse V, King C, Jacobetz MA, et al. Preinvasive and invasive ductal pancreatic cancer and its early detection in the mouse. Cancer Cell. 2003;4(6):437–50. [PubMed: 14706336]
34. McDonnell AM, Robinson BW, and Currie AJ. Tumor antigen cross-presentation and the dendritic cell: where it all begins? Clin Dev Immunol. 2010;2010:539519. [PubMed: 20976125]
35. Krzewski K, Gil-Krzewska A, Nguyen V, Peruzzi G, and Coligan JE. LAMP1/CD107a is required for efficient perforin delivery to lytic granules and NK-cell cytotoxicity. Blood. 2013;121(23):4672–83. [PubMed: 23632890]
36. Daniels TR, Leuchter RK, Quintero R, Helguera G, Rodriguez JA, Martinez-Maza O, et al. Targeting HER2/neu with a fully human IgE to harness the allergic reaction against cancer cells. Cancer Immunol Immunother. 2012;61(7):991–1003. [PubMed: 22127364]
37. Josephs DH, Bax HJ, Dodev T, Georgouli M, Nakamura M, Pellizzari G, et al. Anti-Folate Receptor-alpha IgE but not IgG Recruits Macrophages to Attack Tumors via TNFalpha/MCP-1 Signaling. Cancer Res. 2017;77(5):1127–41. [PubMed: 28096174]
38. Spear S, Candido JB, McDermott JR, Ghirelli C, Maniati E, Beers SA, et al. Discrepancies in the Tumor Microenvironment of Spontaneous and Orthotopic Murine Models of Pancreatic Cancer Uncover a New Immunostimulatory Phenotype for B Cells. Front Immunol. 2019;10:542. [PubMed: 30972056]
39. Nagato T, Lee YR, Harabuchi Y, and Celis E. Combinatorial immunotherapy of polyinosinic-polycytidylic acid and blockade of programmed death-ligand 1 induce effective CD8 T-cell responses against established tumors. Clin Cancer Res. 2014;20(5):1223–34. [PubMed: 24389326]
40. Kim N, and Kim HS. Targeting Checkpoint Receptors and Molecules for Therapeutic Modulation of Natural Killer Cells. Front Immunol. 2018;9:2041. [PubMed: 30250471]
41. Sun H, and Sun C. The Rise of NK Cell Checkpoints as Promising Therapeutic Targets in Cancer Immunotherapy. Front Immunol. 2019;10:2354. [PubMed: 31681269]
42. Xu F, Sunderland A, Zhou Y, Schulick RD, Edil BH, and Zhu Y. Blockade of CD112R and TIGIT signaling sensitizes human natural killer cell functions. Cancer Immunol Immunother. 2017;66(10):1367–75. [PubMed: 28623459]
43. Nunez SY, Ziblat A, Secchiari F, Torres NI, Sierra JM, Raffo Iraolagoitia XL, et al. Human M2 Macrophages Limit NK Cell Effector Functions through Secretion of TGF-beta and Engagement of CD85j. Journal of immunology. 2018;200(3):1008–15.

44. Ferlazzo G, Tsang ML, Moretta L, Melioli G, Steinman RM, and Munz C. Human dendritic cells activate resting natural killer (NK) cells and are recognized via the NKp30 receptor by activated NK cells. The Journal of experimental medicine. 2002;195(3):343–51. [PubMed: 11828009]

45. Sallmann E, Reininger B, Brandt S, Duschek N, Hoflehner E, Garner-Spitzer E, et al. High-affinity IgE receptors on dendritic cells exacerbate Th2-dependent inflammation. Journal of immunology. 2011;187(1):164–71.

46. Pellizzari G, Hoskin C, Crescioli S, Mele S, Gotovina J, Chiaruttini G, et al. IgE re-programs alternatively-activated human macrophages towards pro-inflammatory anti-tumoural states. EBioMedicine. 2019;43:67–81. [PubMed: 30956175]

47. Doris K, Karabela SP, Kairi CA, Simoes DC, Roussos C, Zakynthinos SG, et al. Allergic inflammation does not impact chemical-induced carcinogenesis in the lungs of mice. Respir Res. 2010;11:118. [PubMed: 20796309]

48. Aun MV, Bonamichi-Santos R, Arantes-Costa FM, Kalil J, and Giavina-Bianchi P. Animal models of asthma: utility and limitations. J Asthma Allergy. 2017;10:293–301. [PubMed: 29158683]

49. McMillan SJ, and Lloyd CM. Prolonged allergen challenge in mice leads to persistent airway remodelling. Clin Exp Allergy. 2004;34(3):497–507. [PubMed: 15005746]

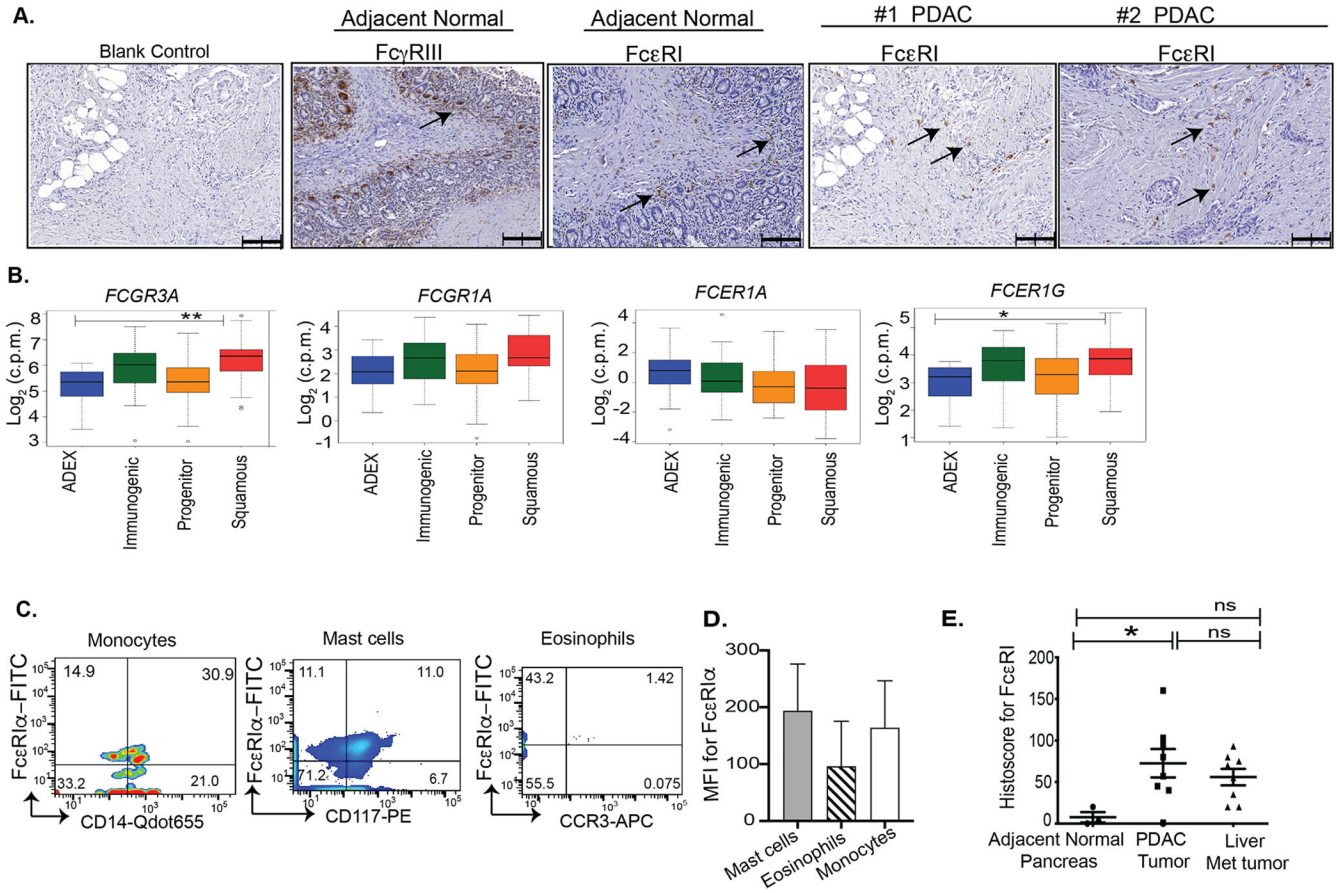

Figure 1. Expression of IgE receptor in pancreatic adenocarcinoma.

A, Representative images show immunohistochemistry staining for FcγRIII and FcεRI (from 2 different patients: #1 and #2) in adjacent normal and pancreatic adenocarcinoma (PDAC) tumor tissues. The scale bar denotes 100μm. **B,** Boxplots depicting *FCER1A, FCER1G, FCGR3A,* and *FCGR1A* expression in different subtypes of PDAC. **C,** Flow cytometer plots depict FcεRIα expression by intra-tumoral $CD14^{+}$monocytes, mast cells, and eosinophils in primary pancreatic tumor tissues. PDAC tumor tissues were digested and prepared into single-cell suspension. Cells were gated on live $CD45^{+}CD3^{-}CD19^{-}CD56^{-}$ immune cells. **D**, Histogram plot display mean fluorescence intensity for FcεRIα on immune cells in human PDAC tumors (n=4). **E**, Histogram plot displays histological score for the quantitation of FcεRIα positive cells in the normal pancreas (n=3), primary pancreatic tumor and matched metastatic liver samples (n=8). Scoring of FcεRI positive cells in IHC was assessed using a formula as described in the method section. Histoscore and box plot data were compared using one-way ANOVA with Tukey's post-hoc test for multiple comparisons. p values: *<0.05, **<0.005.

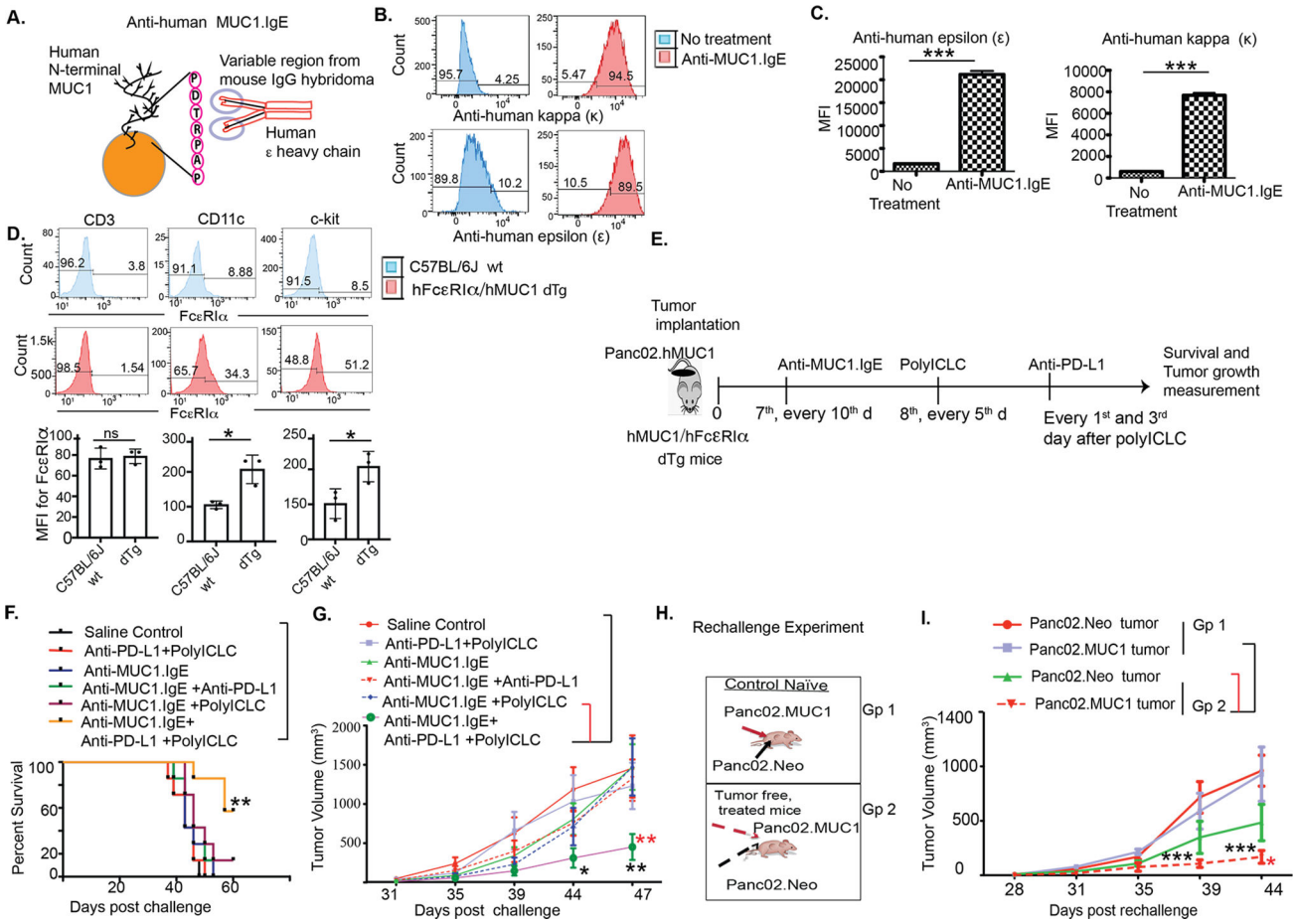

Figure 2. Anti-MUC1.IgE-based immunotherapy reduced tumor burden and prolonged survival in subcute pancreatic tumor-bearing mice.

A, Cartoon depicts anti-MUC1.IgE antibody that recognizes the 'PDTRPAP' region in the N-terminal domain of MUC1 on tumor cells. **B,** Histogram plots demonstrates the binding capacity of anti-MUC1.IgE to the MUC1 expressing Panc02 tumor cells. Binding was determined by immunofluorescence staining of epsilon and kappa chains of anti-MUC1.IgE bound to Panc02.MUC1 cells. **C,** Bar plots represents median fluorescence intensity (MFI) of epsilon (ε) and kappa (κ) chains on Panc02.MUC1 cells. **D,** Histogram plots with corresponding MFI demonstrate FcεRIα expression by T cells, mast cells, and dendritic cells in the blood of mice from different genetic backgrounds. Cells are gated on live cells and fluorescence minus one (FMO) control for FcεRIα was also utilized for the study. **E,** Diagrammatic depiction of the subcute PDAC tumor model followed for dTg mice. The picture represents the day of tumor implantation and treatment regimen with anti-MUC1.IgE (25μg/100μl, i.p.), anti-PD-L1 (200μg/100μl injection, i.p.) and PolyICLC (200μg/100μl injection, i.p.). As mentioned in the picture, treatment began with anti-MUC1.IgE post 7 days of tumor implantation and followed for every 10 days afterwards (a total of 4 doses). PolyICLC treatment began a day after anti-MUC1.IgE and was followed every 5 days (a total of 8 doses). Anti-PD-L1 was given every 1st and 3rd day after PolyICLC (a total of 8 doses). **F,** Kaplan-Meier plots represents percent survival in Panc02.MUC1 subcute tumor-bearing dTg mice in different treatment groups. **G,** Tumor growth curve for indicated

treatment groups in subcute Panc02.MUC1 tumor-bearing mice (n=10). **H,** Cartoon depicts the re-challenge experiments followed for anti-MUC1.IgE + anti-PD-L1 + PolyICLC treated tumor-free and naïve mice. Tumor free (n=6) and naïve mice (n=5) were challenged with Panc02.MUC1 and Panc02.Neo cells on the opposite flanks. **I,** Histogram represents tumor growth curve of Panc02.MUC1and Panc02.Neo tumors in re-challenged dTg mice. Kaplan-Meier curves were compared using Log-rank test; tumor volumes were compared using two-way ANOVA with Bonferroni post-test, p values: *<0.05, **<0.005, ***<0.0005. Red and black asterisks represent the p values of tumor volume between different groups (corresponding to the color in legend). Values are presented as average ± standard error of the mean (SEM), unpaired *t-test* for MFI plots, p value: *<0.05***<0.0005.

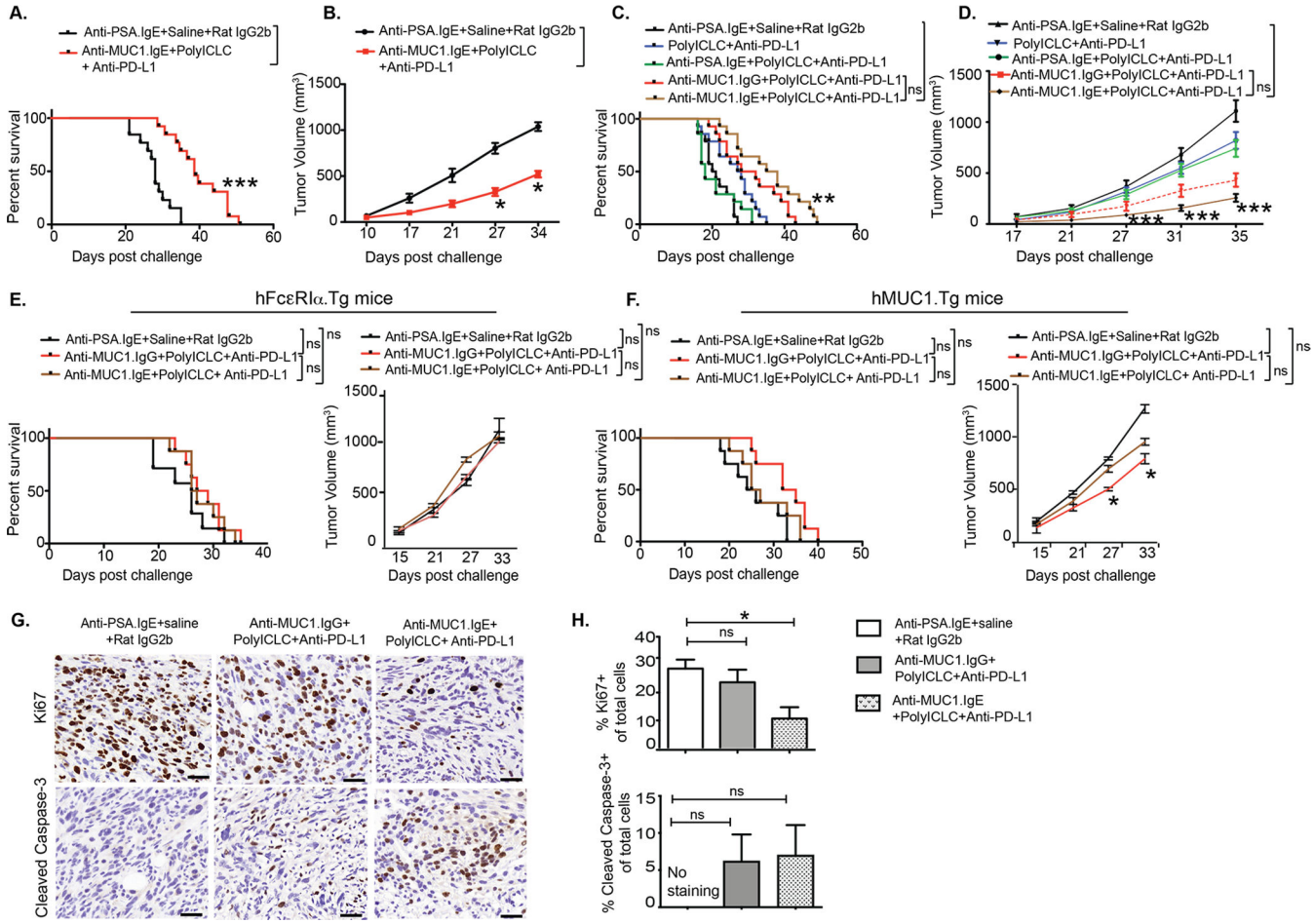

Figure 3. Anti-MUC1.IgE-based immunotherapy relieved tumor burden and prolonged survival of orthotropic pancreatic tumor-bearing mice.

A, Kaplan-Meier plot represents survival of KPC.MUC1 orthotopic tumor-bearing mice in different treatment groups (n=10). **B,** Tumor growth curves for anti-PSA.IgE + RatIgG2b + saline and anti-MUC1.IgE + anti-PD-L1 + PolyICLC in orthotopic tumor-bearing dTg mice. Treatment with anti-MUC1.IgE (25 μg) begin at day 5 and was administer every 5 days afterwards. Treatment dose and schedule for anti-PD-L1 and PolyICLC is same as mentioned for the subcutaneous model. **C,** Kaplan-Meier plot represents survival of KPC.MUC1 orthotopic tumor bearing dTg mice in different treatment groups (n=10). **D,** Tumor growth curves for anti-PSA.IgE + RatIgG2b + saline and anti-MUC1.IgE + anti-PD-L1 + PolyICLC in orthotopic tumor-bearing dTg mice in time-point study. Mice were monitored for tumor volume measurement for 35 days. **E,** Kaplan-Meier plot and tumor growth curves represents survival and tumor volumes for hFcεRIα single Tg mice in different treatment groups (n=8). **F,** Kaplan-Meier plot and tumor growth curves represent survival and tumor volumes for hMUC1 single Tg mice in different treatment groups (n=8). **G,** Representative images demonstrate IHC analysis of Ki67 (proliferation marker) and cleaved Caspase-3 in the tumor sections from different treatment groups. **H,** Histogram plots demonstrate quantification of Ki67 and cleaved caspase-3 positive cells as percentage of total cells in each tumor section (n=4). The scale bar denotes 20μm. Kaplan-Meier curves

were compared using Log-rank test; tumor volumes were compared using two-way ANOVA with Bonferroni's post-test, *p* value: *<0.05, ***<0.0005, ***<0.0005. IHC data represents analysis of 4 mice/group by one-way ANOVA with Tukey's post hoc test, *p* value: *<0.05.

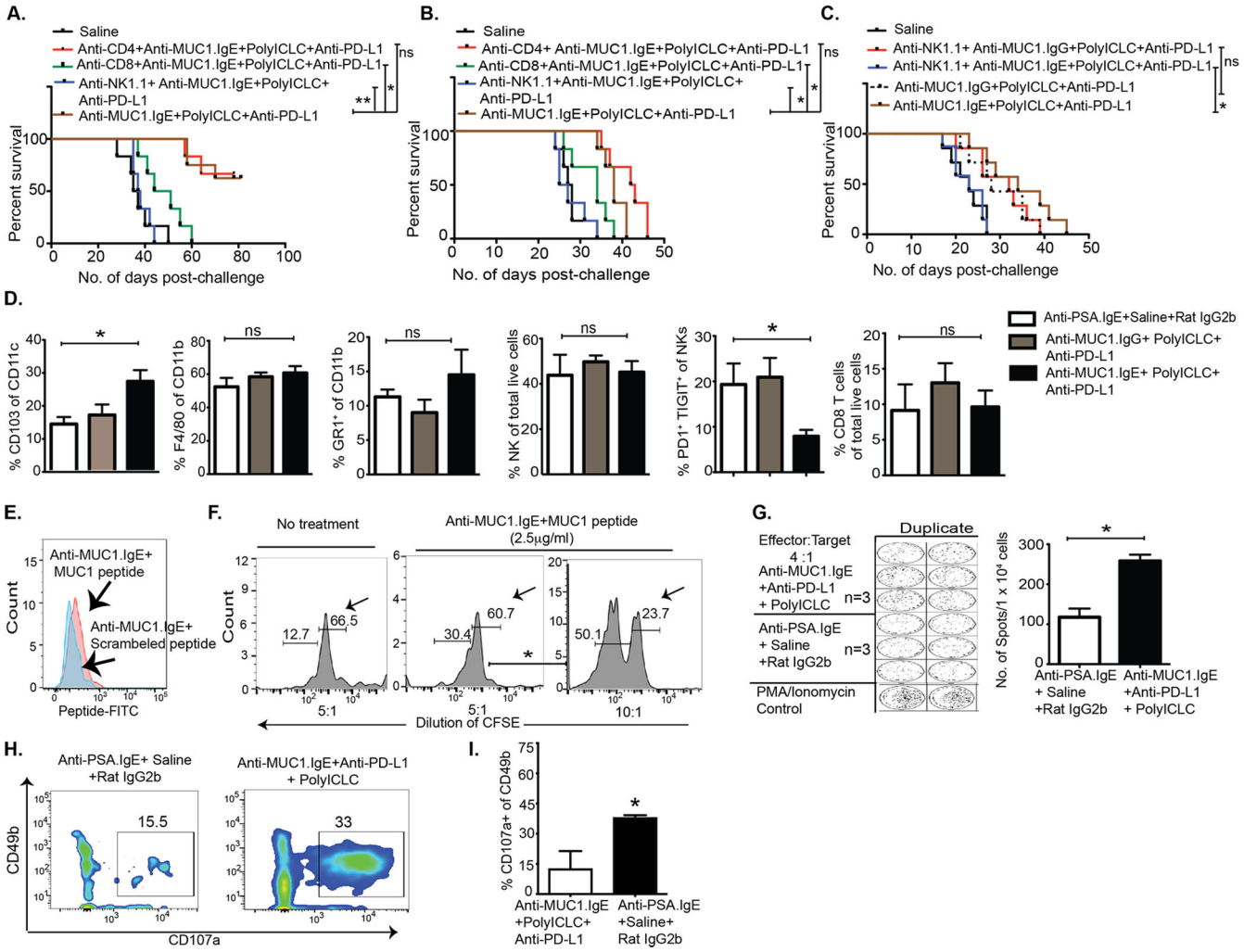

Figure 4. NK and CD8 T cell depletion abrogated efficacy of anti-MUC1.IgE-based combination.

A-B, Kaplan-Meier plots represent survival of Panc02.MUC1 subcutaneous (**A**), and KPC.MUC1 orthotopic tumor-bearing dTg mice (**B**) in the presence and absence of CD4, CD8, and NK cells in different treatment groups (n=6). Depletion of NKs, CD4, and CD8 T cells was achieved by treatment with anti-NK1.1 (100 μg), anti-CD8 (200 μg), and anti-CD4 (200μg) at days −6, −2, 0, +2, +6, +15, and +25; (day 0 is tumor implantation). Treatment with antibodies for subcutaneous and orthotopic study is mentioned in previous section. **C,** Kaplan-Meier plot displays survival of KPC.MUC1 orthotopic tumor-bearing mice treated with anti-MUC1.IgE-based and anti-MUC1.IgG-based combination with or without NK cell depletion (n=7). **D,** Bar graph shows the for $CD103^+$ DC (of total CD11c), macrophages, $GR1^+$ (of total $CD11b^+$ cells), NK ($CD335^+$ $CD3^-$) and CD8 T cells (of total live cells), and PD-$1^+$$TIGIT^+$ NK (of total NKs) in the tumors from different treatment groups (n=5). Mice were monitored for tumor-volume measurement for 35 days. On day 35, freshly harvested tumor sample were assessed for TIL analysis using flow cytometer. **E**, Antigen-antibody complex (MUC1 peptide-anti-MUC1.IgE) uptake by splenic DCs from anti-MUC1.IgE-based combination treated dTg mice. MUC1 or scrambled peptide-FITC were used for the study. **F,** CFSE-based CD8 T-cell proliferation in the presence and

absence of antigen-antibody loaded DCs post 3-day co-culture at different ratio. **G,** ELISpot images and quantitation for the activity of splenic CD8 T cells from treated mice against KPC.MUC1 tumor cells (n=3). **H,** Contour plots represents CD107a positive NKs from treated tumor-bearing mice in *ex vivo* assay. Splenic NKs were harvested from treated tumor-bearing mice, cultured in the presence of KPC.MUC1 (10:1 co-culture ratio), and treated with the respective combination. **I,** Histogram presents quantitation of percent degranulated NKs of total NK in CD107a-based degranulation assay. Kaplan-Meier curves were compared using Log-rank test; frequency of different immune subsets in treated tumor was compared using one-way ANOVA with Bonferroni post-test. Values are presented as average ± SEM, unpaired *t-test* for ELISpot and degranulation assay, p values: *<0.05.

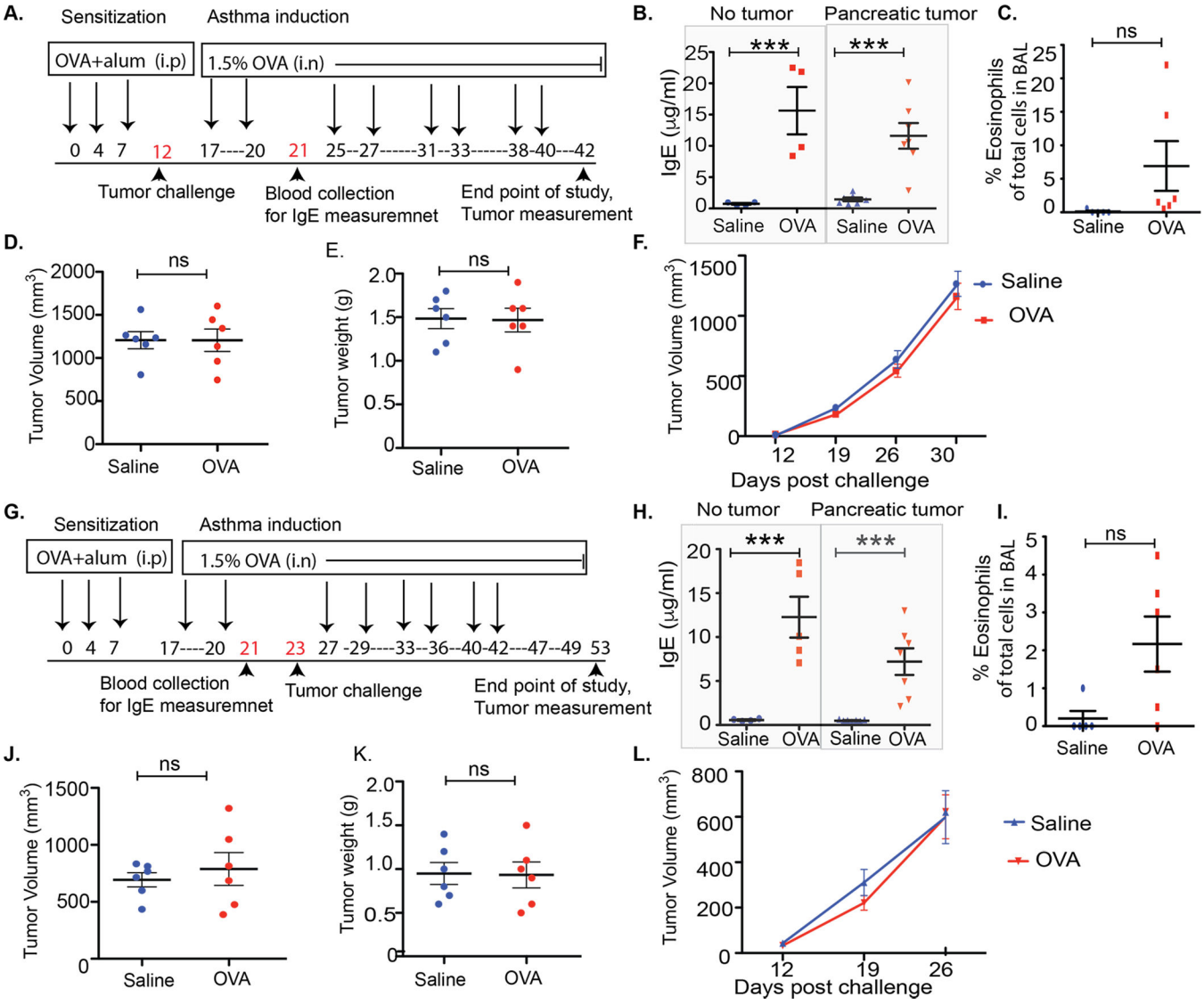

Figure 5. OVA-induced IgE did not attenuate pancreatic tumor growth in early and late stage tumor models.

A, Schematic presentation of early OVA-tumor model where KPC tumor cells (5×10^3) were implanted orthotopically in mice before the beginning of OVA aerosol challenges in mice. Mice sensitized and challenged with saline served as control. Mice that were sensitized and challenged with OVA but with no tumor implantation served as another control to account for the effect of tumor cells on serum IgE levels. **B,** Dot plots show serum IgE levels in different groups. **C,** Dot plots show differential count of eosinophils in the BAL fluid from mice in different groups. **D-E**, Dot plots show tumor volume (**D**) and weight (**E**) in tumor-bearing mice in early-OVA tumor model. **F**, Tumor growth curves for OVA and saline challenged mice. Tumor volume was measured using ultrasonography every week. **G,** Schematic presentation of late ova-tumor model where KPC tumor cells were implanted orthotopically in mice after 1 cycle of OVA aerosol challenges. Mice sensitized and challenged with saline served as control. Mice sensitized and challenged with OVA but with no tumor implantation served as another control to account for the effect of tumor cells

on serum IgE levels. **H**, Dot plots show serum IgE levels in different groups. **I,** Dot plots show differential count of eosinophils in the BAL fluid from mice in different groups. **J-K**, Dot plots show tumor volume (**J**) and weight (**K**) in tumor-bearing mice in late-OVA-tumor model. **L**, Tumor growth curves for OVA and saline challenged mice. Tumor volume was measured using ultrasonography every week. IgE levels, tumor growth, and tumor volume were compared between groups using unpaired *t-test*. Values are presented as average ± SEM. Tumor growth curve was analyzed using two-way ANOVA with Bonferroni post-test for tumor volume, *p* values: *<0.05, **<0.005, ***<0.0005.

Table 1:

List of oligonucleotide primers

Target	Name	Nucleotide sequence of primers	Product size
Fcer1a	hFcεRIα-FP	5'-AGT CAG TCT TGA ATG GCT TCC TG-3'	444bp
	hFcεRIα-RP	5'-TCT TCG TCC CAT CAC TTC TGC TT-3'	
Muc1	hMUC1-FP	5'-GTA TCG GCC TTT CCT TCC CCA T-3'	236bp
	hMUC1-RP	5'-ACC TTA AGT GCA CCA GTC CCT C-3'	

Table 2:

List of antibodies

FACS antibodies	Clone	Cat no:	Vendor
Human			
Anti-CD3-PerCP710	OKT3	46-0037-42	eBioscience, Inc.
Anti-CD45-APC780	APC780	47-0459-42	eBioscience, Inc.
Anti-CD19-PerCP710	SJ25C1	46-0198-42	eBioscience, Inc
Anti-CD56-PerCP710	HCD56	46-0567-42	eBioscience, Inc
Anti-CD11b-PE-CY7	ICRF44	25-0118-42	eBioscience, Inc
Anti-CD11c-Alexa700	3.9	56-0116-42	eBioscience, Inc
Anti-CD117-PE	YB5.B8	12-1179-42	eBioscience, Inc
Anti-CCR3-APC	5E8-G9-B4	310708	Biolegend, Inc.
Anti-CD15-Alexa 700	W6D3	323026	Biolegend, Inc.
Anti-CD14-Qdot 655	61D3	Q10056	Invitrogen, Inc.
Anti-Fcer1A-FITC	AER-37	334608	Biolegend, Inc.
Anti-CD16-605 NC	CB16	93-0168-42	eBioscience, Inc.
Anti-CD49d-PE-CY	9F10	304314	Biolegend, Inc.
Anti-human IgE FC-FITC		H15701	Thermo Fisher Sceintific, Inc.
Anti-human Kappa-APC	TB28-2	34118	BD Bioscience, Inc.
Mouse			
Anti-CD103-BV605	2E7	121433	Biolegend, Inc.
Anti-TIGIT-BV421	1G9	142111	Biolegend Inc.
Anti-CD3-PerCP	145-2C11	100326	Biolegend Inc.
Anti-F4/80-PE	BM8	123110	Biolegend Inc.
Anti-CD11b-eFlour450	M1/70	48-0112-82	Biolegend Inc.
Anti-CD11C-AF700	N418	117320	Biolegend Inc.
Anti-CD107a-PE/CY7	1DB4	121620	Biolegend Inc.
Anti-Gr-1-APC	RB6-8C5	108440	Biolegend Inc.
Anti-CD335-PE/CY7	29A1.4	137618	Biolegend Inc.
Anti-PD-1-APC	RMP1-30	109111	Biolegend Inc.
Anti-CD8-APC-AF750	53-6.7	27-0081-82	eBioscience Inc.
Anti-CD4-APC/CY7	GK1.5	100413	Biolegend Inc.
Anti-CD49b-APC fire 750	DX5	108926	Biolegend Inc.
Anti-NKG2D-PE	C7	115705	Biolegend Inc.
anti-c-kit-APC	2B8	105812	Biolegend Inc.
IHC antibodies			
Anti-Ki67	SolA15	14-5698-92	Thermo Fisher Sceintific, Inc.
Cleaved Caspase-3		9661T	Cell Signaling Technologies, Inc
Anti-FCGR3	3G8	LS-C204310	LifeSpan BioSceinces, Inc.
Anti-FCER1a	9E1	LS-B3150	LifeSpan BioSceinces, Inc.
Mice treatment			
Anti-PD-L1	10F.9G2	BE0101	BioXcell, Inc.